Bioinspired Long-Wavelength Excitable Near-Infrared AIEdots for Endometriosis Targeting and Image-Guided Surgery

Huashan Zhao,[†,#] *Chunbin Li,*[‡,§,#] *Wen Zhu,*[†,#] *Ming Yu,*[†] *Binbin Huang,*[†] *Xiaopeng Wang,*[§] *Jingwei Li,*[†] *Yali Yang,*[†] *Li Xue,*[†] *Jen-Shyang Ni,*[£] *Xiaohua Lei,*[†] *Pei-Gen Ren,*[†] *Pengfei Zhang,*[‡,*] *Jianguo Wang*[§,*] *and Jian V. Zhang*[†,*]

[†]Center for Energy Metabolism and Reproduction, Shenzhen Institutes of Advanced Technology, Chinese Academy of Sciences, Shenzhen 518055, China.

[‡]Guangdong Key Laboratory of Nanomedicine, CAS Key Laboratory of Health Informatics, Shenzhen Bioactive Materials Engineering Lab for Medicine, Institute of Biomedicine and Biotechnology, Shenzhen Institutes of Advanced Technology, Chinese Academy of Sciences, Shenzhen 518055, China.

[§]College of Chemistry and Chemical Engineering, Inner Mongolia Key Laboratory of Fine Organic Synthesis, Inner Mongolia University, Hohhot 010021, China.

[£]Department of Biomedical Engineering, Southern University of Science and Technology (SUSTech), Shenzhen 518055, China; Department of Chemical and Materials Engineering, Photo-sensitive Material Advanced Research and Technology Center (Photo-SMART), National Kaohsiung University of Science and Technology Kaohsiung 80778 (Taiwan), China.

#These authors contributed equally to this work.

*Correspondence should be addressed to Pengfei Zhang, Jianguo Wang and Jian V. Zhang.

E-mail: pf.zhang@siat.ac.cn; wangjg@iccas.ac.cn; jian.zhang@siat.ac.cn

Abstract

Endometriosis（EM）is a non-cancerous and intractable disease in clinic due to the ambiguity of its etiology and mechanism. Surgical removal of the lesions is more efficient method for EM treatment compared with pharmacological intervention. Intraoperative identification of the endometrial ectopic sites is a prerequisite, however, available probes with high specificity remain limited, owing to lack of specific biomarkers. Here, based on a polypeptide derived from VAR2CSA protein (CSA) and a near-infrared AIE material (TPA-TBZ-2), we prepared a CSA AIEdots capable of labeling the EM lesions by a one-step nanoprecipitation method. The nanodots have an absorbance maximum at 610 nm with a wide emission range from 650 to 850 nm and an absolute quantum yield of up to 34% in the aggregation states. Through *in vitro* assay, the dots could specifically label endometrioid cells (Ishikawa cells), and flow cytometry experiments showed its specific spectral absorption peak, compared with empty particles and scrambled peptide groups. Next, to verify the ability of the dots to label the ectopic endometrium *in vivo*, we established a mouse model of endometriosis. After injection the dots into model mouse intravenously for 24 hours, the AIE signaling could be specifically detected at the ectopic lesions in an IVIS small animal imaging system. The CSA AIEdots were further used for image-guided EM resection *in vivo* and showed a high EM-to-normal tissue signal ratio. Taken together, our AIE nanodots-based EM diagnosis system is a promising candidate for EM development monitoring and surgical navigations.

Keywords: Endometriosis; Near-infrared fluorescence; Aggregation-induced Emission; Nanoparticles; Image-guided surgery

1. Introduction

Endometriosis (EM), a debilitating and excruciating disease, refers to the abnormal growth and survival of active endometrial cells outside the endometrium including pelvic tissues and adjacent organs, with features of chronically gynecological inflammation [1], which would lead to various diseases such as dysmenorrhea, irregular menstruation, infertility and endometrioid ovarian cancer [2], with an incidence of up to 10% [3]. Its pathogenesis has not been elucidated yet, although there are some hypotheses involved in endocrine factors, inflammation, immunity, neovascularization, genetic factors, stem cell theory and so on [4]. Among them, the retrograde menstruation theory is classic theory about the formation of abdominal EM [5]. Endometrial stromal cells through the peritoneal cells, especially the peritoneal extracellular matrix, complete adhesion, invasion, angiogenesis and formation of ectopic lesions [6]. The treatment of EM mainly include medical therapy and surgical removal. However, due to the ambiguity of mechanism, medical option only relieve symptoms such as pain rather than radical therapy of EM [7]. Comparatively, surgical treatment is widely accepted to be more efficient for EM therapy [7]. Although laparoscopy is the “gold standard” for definitive diagnosis of EM [8], it is based on large morphological abnormalities to make judgment [9, 10], which is difficult to define the lesions, especially at early stage, and hardly to recognize or remove lesions conveniently and effectively. Recently, near-infrared fluorescence (NIRF) imaging technique, providing real-time information about the operating field without ionizing radiation and complex infrastructure, shows great potential for image-guide surgery to excise tumors accurately. However, there were very little reports on fluorescence imaging-guided surgery of EM.

Rapidly expanding field of image-guided surgery needs new materials for near-infrared imaging with deep tissue penetration, high brightness and good stability. With the development of nanotechnology, fluorescence nanomaterials, especially with emission in range of near-infrared spectrum provide excellent candidates for real-time monitoring of surgical procedures with high spatio-temporal resolution and sensitivity [11]. Inorganic nanomaterials, such as semiconductor quantum dots, lanthanide-doped upconversion nanoparticles and noble-metal nanoparticles, exhibited outstanding photostability and brightness, presenting great opportunities for longer-term *in vivo* tracking and imaging. Unfortunately, most fluorescent inorganic nanoparticles are composed of highly toxic heavy metal cations, which raises the concerns of long-term toxicity and limits the further clinical transition [12]. In terms of biocompatibility, the organic nanodots derived from the nanoaggregate of luminescent small molecule or polymers are generally considered more favorable than the inorganic nanoparticles [13]. However, these organic nanodots suffer from a fundamental problem: the molecules or polymers are packed together so closely that they can be affected by aggregation caused quenching, in which most of the energy coming from the original light source is quickly dissipated and fails to trigger fluorescence. As a result, the brightness of as-prepared organic nanoparticles tends to decrease along with the increase of molecules or polymers doping concentration, which presents a dilemma for fabricating highly bright and photostable organic nanoparticles. A fundamental solution was pioneered in 2001, Tang et al proposed an aggregation-induced emission (AIE) conception. The luminogens with AIE property (AIEgens) are non-emissive in solutions but become highly fluorescent upon aggregate formation because the restriction of the intramolecular rotations (RIR), which make them ideal candidate materials for preparation of highly bright and photostable organic fluorescent nanoparticles. Since the

first report of development of organic dots with aggregation-induced emission (AIE dots) for bioimaging, numerous reports suggest that these biocompatible highly bright nanoparticles have the potential to improve conventional therapeutic and imaging capability for disease detection and treatment [14-18]). For instance, Liu's group produced the NIR AIE nanoparticles for image-guided tumor resection [19]. Ding's group developed NIR afterglow luminescent AIE nanoparticles for precise image-guided cancer surgery [20, 21]. Tang's group reported NIR-II AIE dots for intraoperative identification of ureters during abdominal and pelvic surgeries. [22]. However, to the best of our knowledge, until now, there were no report on using AIE nanoparticles for fluorescence image guidance in EM resection.

The accumulating evidence suggest that nanomedicine can shift the current paradigm for diagnosis and treatment of EM [23, 24]. And active targeting is much more reliable compared with passive targeting (EPR effect) in aspect of increasing retention and accumulation of nanoparticles in EM lesions, which is achieved by modification of nanoparticles with targeting ligands (such as peptides, antibodies and small molecules) that can bind specific receptors expressed on target cells and facilitate internalization of the modified nanoparticles by these cells [23, 25-30]. As to binding peptide, we focused on a VAR2CSA protein-derived CSA-binding peptide. The rationale lies in that the malaria parasite *Plasmodium falciparum* replicates within infected erythrocytes (IEs) could effectively sequester in the placental intervillous spaces of a pregnant woman. Placental adherence is mediated by the malarial VAR2CSA protein exposed on the IE membrane [31], which shows high affinity to Chondroitin sulfate A, one of the most abundant glycosaminoglycan in the human placenta [32-35]. Previously, our group has demonstrated that VAR2CSA protein-derived CSA-binding peptide could be used as

targeting ligand for placenta-specific drug delivery [36]. Based on adherent property of this CSA-binding peptide to abnormal or adhesive tissue, we hypothesized this targeting ligand would identify the EM lesions.

In this work, we developed a donor–acceptor (D–A) structural thiadiazolobenzotriazole (TBZ)-cored NIR emissive AIEgen. As-prepared AIEgen were encapsulated in clickable lipid micelle to produce biorthogonal NIR AIEdots with long excitation wavelength (610 nm) and large Stokes (172 nm) shift. The CSA-binding peptide derived from VAR2CSA malaria protein was decorated on the surface of AIE nanoparticles by click chemistry for effectively targeting endometrial stromal cells and image-guided EM resection. It should point out that this is the first trail of AIE nanoprobes for gynecological disease treatment.

2. Results and Discussion

Two thiadiazolobenzotriazole-cored NIR molecules, TPA-TBZ-1 and TPA-TBZ-2 were easily synthesized and purified by undergoing the route depicted in Figure S1 (Supporting Information), with a high yield of 80-92%. All chemical structures were characterized and confirmed by NMR and high-resolution mass spectrometry (HRMS) (Supporting Information). In these molecules, thiadiazolo-benzotriazole (TBZ, green) with or without alkyl (red) as the acceptor and triphenylamine (TPA, blue) as the donor to form strong donor-acceptor-donor (D-A-D) interaction, which could facilitate the intramolecular charge transfer (ICT) and conjugation length. As shown in Figure 1A, 1D, UV-Vis absorption of TPA-TBZ-1 and TPA-TBZ-2 in dimethylsulfoxide solution (DMSO) were investigated, which exhibited a much broad absorption spectra covering from 300-800 nm, respectively, where the former one absorption

bands centered at 340 and 610 nm, and the latter one absorption maxima at 340 nm and 594 nm. Furthermore, the efficient PL spectra of TPA-TBZ-1 and TPA-TBZ-2 covering from 650-850 nm, where the maximum emission features respectively located at 782 nm and 718 nm, finally ensure that most of the spectra is located in the NIR window (700–900 nm) for signal collection. By comparing their maximum excitation and emission wavelength, TPA-TBZ-2 exhibited more remarkably Stokes shift (172 nm), longer excitation and emission wavelength (Figure 1), which is favorable for achieving high contrast for *in vitro* and *in vivo* imaging applications. Then, the AIE property of TPA-TBZ-2 were confirmed by studying its PL spectra in water/DMSO mixtures with different water volume fractions (Figure 1B) and plots of PL intensity in the mixed solvents were also curved in Figure 1C. The PL intensity of TPA-TBZ-2 decreased gradually with water fraction lower than 10%, accompanied with spectral red-shifts, could cause by the twisted intramolecular charge transfer (TICT) effect. When water fraction exceeds 10 %, the addition of water would induce the formation of aggregates, and the PL intensity intensified largely, showing the unique AIE characteristics. In contrast, the PL intensity of TPA-TBZ-1 quickly decreased when the water fraction increased gradually (Figure 1E, F), and displayed lower fluorescence intensities in aggregates than in pure DMSO solution, finally almost no fluorescence, possessing ACQ characteristics similar to traditional dyes. Of note, TPA-TBZ-1 exhibited different optical properties because of the different electron-withdrawing groups whose acceptor with alkyl chain, which could be ascribed to the twisted molecular skeleton.

In order to assess the molecular conformation effect, density functional theory (DFT) calculations were performed at B3LYP/6-31G*(d) level for TPA-TBZ-1 and TPA-TBZ-2. As

depicted in Figure 2, the highest occupied molecular orbital (HOMO) of two molecules is distributed in both donor and acceptor units, while the separated spin densities of lowest unoccupied molecular orbital (LUMO) are mainly located in TBZ core, suggesting the existence of obvious intramolecular D-A interaction and efficient ICT effect from TPA to TBZ. Moreover, the large energy gap for TPA-TBZ-1 between HOMO and LUMO is 2.12 eV than that for TPA-TBZ-2 (1.88 eV), resulting in the absorption wavelength was redshifted, which is also well in accordance with the result in Figure 1A and 1D.

As above mentioned that TPA-TBZ-2 exhibited a long excitation wavelength (>600 nm) and excellent AIE properties, which could be a promising candidate for further bioimaging applications (Figure 3A). As shown in Figure 3B and Figure S3, the endometrium-specific NIR AIEdots (CSA AIEdots) were prepared by one-step nanoprecipitation method using TPA-TBZ-2 as luminogen and DSPE-PEG and DSPE-PEG-DBCO as encapsulation matrices, where DSPE intertwined with TPA-TBZ-2 to form the hydrophobic core, and the hydrophilic PEG segment self-assembled to form the outer layer with DBCO functional groups on surface. CSA-N_3 (an azido-modified polypeptide derived from VAR2CSA protein) was mixed and decorated on NIR AIEdots through biorthogonal click conjugation during the nanoprecipitation process. Then, UV-Vis absorption and PL spectra for CSA AIE dots was measured was shown in Figure 3B. The broad absorption spectra covering from 300-800 nm and two absorption bands centered at 340 and 610 nm, where the former is assigned to π-π^* and n-π^* transitions of the conjugated aromatic skeleton while the latter is attributed to the intramolecular charge transfer (ICT) from TPA units to TBZ core. Contract to reported AIE dots, the absorption maxima both one was located in the 500-700 nm range and the peak wavelength at 610 nm was rate, which is favorable

for averting the self-absorption tissue. Furthermore, the PL maximum show a large emission range with strong fluorescence mainly located in NIR region, which was more suitable for *in vivo* fluorescence imaging. Interestingly, the CSA-binding peptide-decorated AIEdots showed blue-shifted emission maxima (760 nm versus 782 nm) and slightly smaller Stokes shifts (150 nm versus 172 nm) than that in DMSO solution. The morphology and size of the AIEdots were investigated by using dynamic light scattering (DLS) and transmission electron microscope (TEM). As suggested in Figure 3B, CSA AIEdots revealed hydrodynamic diameter of about 67 nm by DLS measurement, while TEM images exhibited a kind of monodispersed nanosphere with an average diameter of about 100 nm (Figure 3C). Both of the photos and DLS measurements of nanoparticle dispersion in water under white light irradiation suggested it without any precipitation in solution for 15 days, indicating the long shelf time of CSA AIEdots (Figure 3D). In addition, the obtained CSA AIEdots clearly demonstrated excellent photostability compared with traditional NIR fluorescent dye (Cy5), which is unaltered even under continuous exposure with 610 nm excitation light within 30 min (Figure 3E). These results indicated that as-prepared bright NIR AIE nanoparticle offer great potentials for bioimaging.

Chondroitin is a natural biomarker with immense biomedical applications [37]. Chondroitin sulfate A is usually correlated with adhesion of tissue [29]. CSA-binding peptide derived from VAR2CSA protein, a 350 kD protein containing six Duffy-binding like DBL domains expressed by erythrocytes after infection of by the malaria parasite Plasmodium falciparum, shows high affinity to chondroitin sulfate A in the tissue with abnormal adhesion [38, 39]. Based on our previous works and the reports from other groups [36, 40-42], we

speculate some chondroitin sulfate, including chondroitin sulfate A, might be potential marker for EM due to its abnormal adhesion property. The binding of CSA AIEdots to the ishikawa cells (human endometrial cells) was visualized by using confocal microscopy imaging. Ishikawa cells treated with CSA AIEdots showed strong NIR fluorescence intensity on the cell surface. However, the ishikawa cells treated with SCR AIEdots (AIEdots decorated with disordered peptides) or bare AIEdots showed negligible fluorescence signals on the cell surface. To confirm the specificity of as-prepared AIEdots, negative cells line (293 cells, human renal epithelial cells) was used as control and almost no signal is captured on the cells incubated with different nanoparticles (Figure 4A), revealing that the function of peptide could well retained through biorthogonal conjugation and as-prepared CSA AIEdots could distinguish endometrial cells from other cells through the specific targeting ability of CSA-binding peptides (Figure 4A). Moreover, similar results were validated again via flow cytometry assay (Figure 4B), in which only the endometrial cells treated with CSA AIEdots showed stronger fluorescence compared with the control groups under 640 nm excitation. Meanwhile, the cell viability of as-prepared AIE dots with concentration ranging from 0 μg/ml to 5 μg/ml was evaluated using CCK8 (Cell Counting Kit-8) method. The results revealed negligible cytotoxicity after 24 h incubation (Supporting Information), which indicated as-prepared AIEdots were biocompatible for further *in vivo* imaging applications.

Further, *in vivo* endometrium-specific targeted imaging was also evaluated by intravenous injection of the nanoparticles into EM model mice, whose EM lesion sites possessed higher chondroitin sulfate A level than normal mice (Figure 5A). Eight-week-old C57 female mice were anesthetized with Avertin. Part of one side of uterus was removed and cut off into 2 mm

X 2 mm pieces. Then the 3 pieces of uterus tissue containing endometrium were auto-transplantated into mesenterium nearby vessel, fixed with 10-0 suture. With the recovery of mouse for 1 month, the EM lesions could formed. After CSA AIEdots delivered systemically for 24 hours, the fluorescence signal was almost located around the EM lesion site. By contrast, in the case of mouse treated with SCR AIEdots, AIE dots or PBS buffer, the fluorescence signal only appeared in liver, as it has been widely accepted that nanoprobes could easily be enriched in reticuloendothelial system organs (such as liver and spleen). The clearer AIE signals processed by CSA AIEdots could be detected compared with control groups in the abdomen when skin and abdominal wall were removed, which could be more convenient for the EM surgery treatment (Figure 5B-E). Then, the EM sites were isolated by virtue of specific fluorescent signals, simulating clinical surgery to remove the lesions, due to applicable contrast to the adjacent intestine tissue that showed negative labeling (Figure 5F-I), while there were no obvious signaling change among different groups in other main organs (heart, lung, kidney, liver and spleen) (Supporting Information). Furthermore, after tissue section and immunostaining with endometrial stromal cell marker (vimentin), we found the positive cells labeled by CSAAIE dots colocalized to the vimentin positive cells compared with control group (Supporting Information), indicating the specificity of CSA AIEdots to EM site.

To further investigate the potential toxicology of CSA AIE dots *in vivo*, healthy C57 mice were intravenously administrated with CSA AIE dots (500 μg/mL) as well as untreated healthy mice. The mice were sacrificed on 24h post injection and the main organs of mice in each treatment group were excised and sectioned for H&E staining, and there were also no pathological change charged (Supporting Information). The serological test indicated CSA

AIEdots had no evident effect on the function of liver, kidney and heart (Supporting Information).

3. Conclusion

In summary, we developed a new D-A typed highly bright AIEgen TPA-TBZ-2 was developed. This biocompatible AIEgen does not only exhibit an excellent absorptivity but also displays good fluorescence signals in the NIR region. Furthermore, EM stromal cells -targeting NIR AIEdots was developed by decoration of 28-mer peptide derived from VAR2CSA malaria protein through click chemistry. As-prepared nanoprobes could specifically accumulate in EM stromal cells for image-guided lesion resection. This work paved the way to using AIE-based nanoprobes for gynecological disease diagnosis and treatment.

Figure legends

Figure 1 Comparison of AIE properties

A) The absorption wavelength of TPA-TBZ-2. B) The fluorescence spectrometer results of TPA-TBZ-2. C) The peak graph of panel B with change of the water content. D) The absorption wavelength of TPA-TBZ-1. E) The fluorescence spectrometer results of TPA-TBZ-1. F) The peak graph of panel E with change of the water content.

Figure 2 Density functional theory calculations

Calculations for TPA-TBZ-1 and TPA-TBZ-2 at B3LYP/6-31G*(d) level.

Figure 3. Preparation of CSA AIE dots

A) Synthesis diagram of CSA AIEdots. B) Excitation and emission spectrum characterization of AIEdots with TPA-TBZ-2. C) Size measurement of AIEdots with TPA-TBZ-2. D) Precipitation stability of TPA-TBZ-2 within 14 day. E) Optical stability detection under 610 excitation light continuous exposure. The CY5 served as control.

Figure 4. *In vitro* analysis of CSA AIEdots for cell binding

A) Fluorescent detection of AIE signals in Ishikawa cells by CSA AIEdots. The cells could be labeled by the dots in cytoplasm, compared with scrambled control (SCR AIEdots) and nanoparticle without the CSA peptide decoration (AIEdots). The inserts at top left corner was

amplification of the positive cells indicated by the arrow. Whereas the labeling test by CSA AIEdots using 293 cell line was as control. Scale bar: 50 μm. B) The cytometric assay of the CSA AIEdots. The ishikawa cells treated by CSA AIEdots showed more fluorescence level compared with scrambled and nanoparticle control group. The cytometric assay of the CSA AIEdots using 293 cell line was as control.

Figure 5. EM model establishment and *in vivo* EM targeting imaging and surgery

A) Schematic diagram of EM model. B) Live imaging under IVIS system after IV injection of PBS (PBS: 1) and dots (AIEdots: 2, SCR AIEdots: 3 and CSA AIEdots: 4). B-E) The imaging before and after the viscera exposure by removing the skin and abdominal wall. F-I) The local enlarged images and dissected EM lesions under light field and IVIS system.

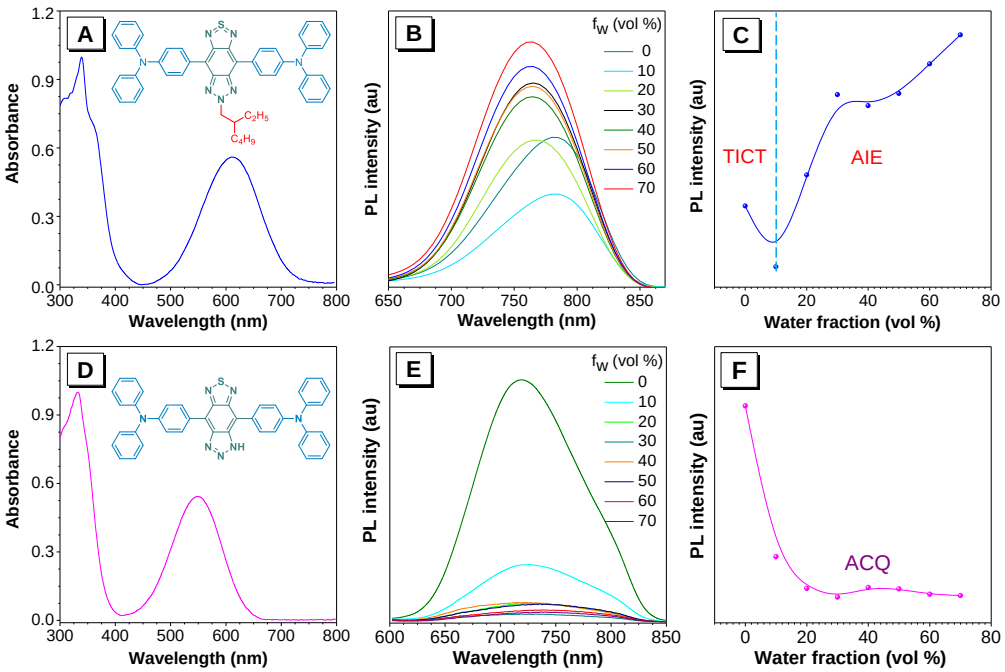

290

291 **Figure 1**

292

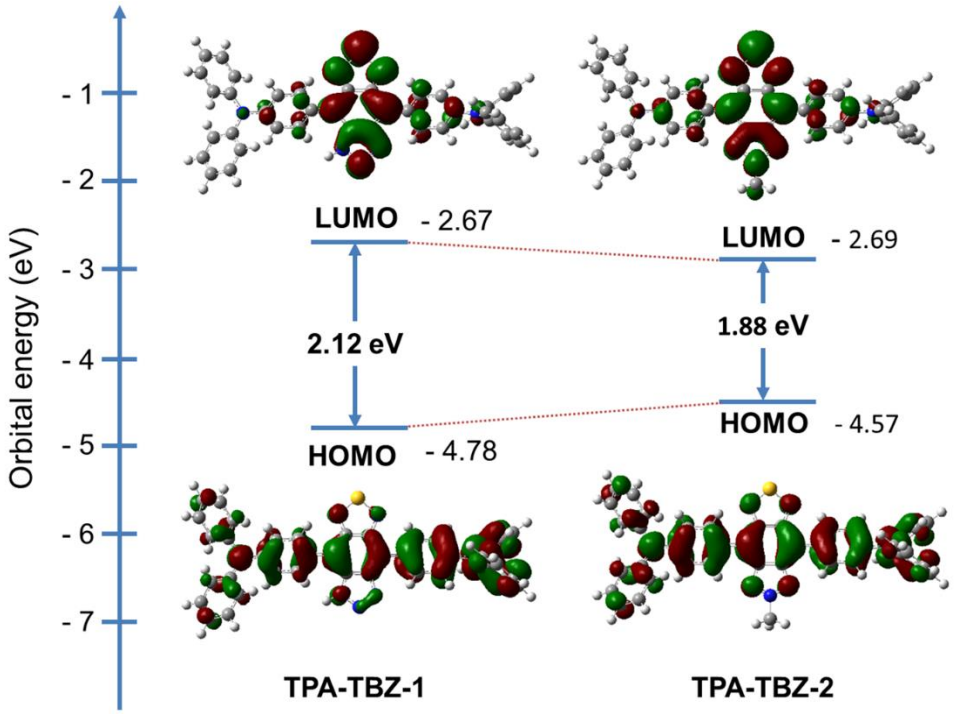

293

294 **Figure 2**

295

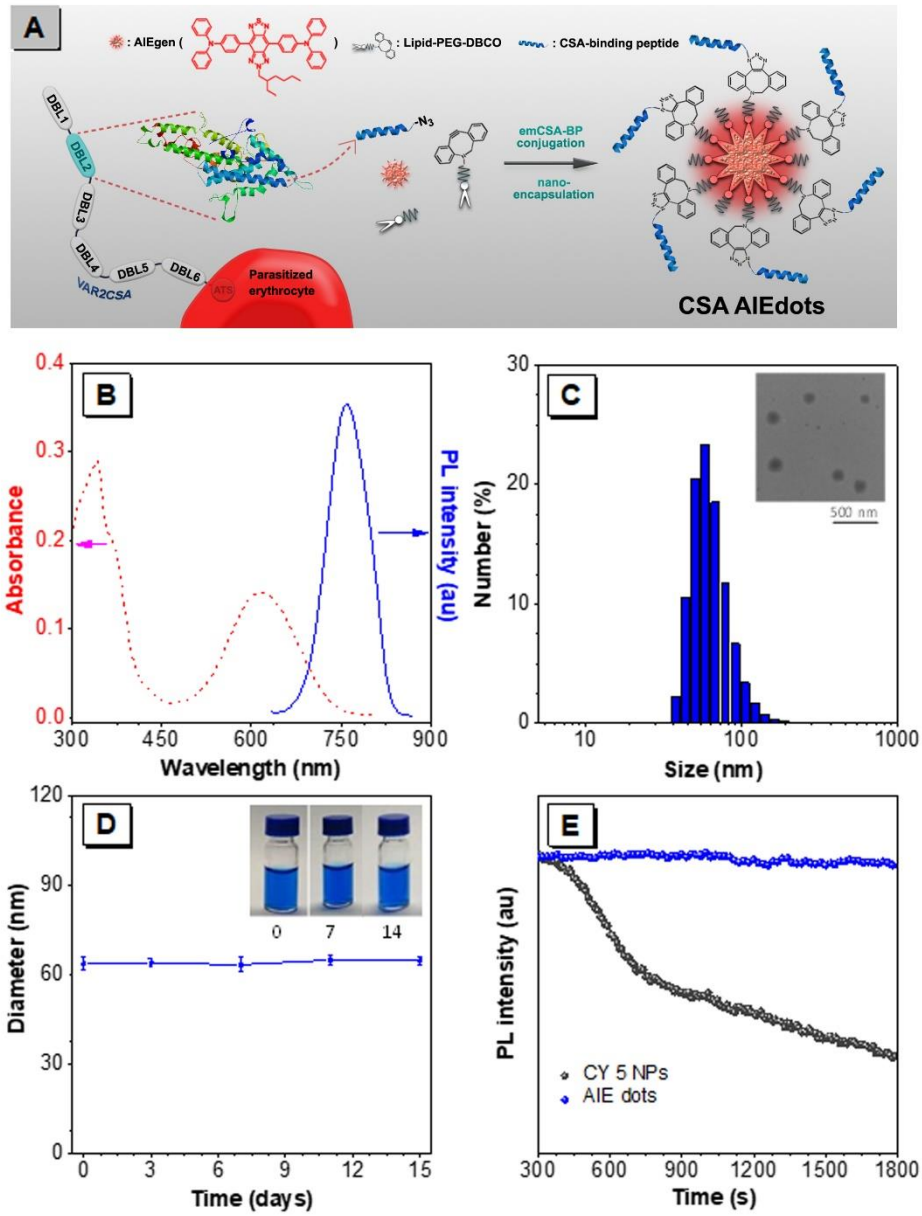

296

297 **Figure 3**

298

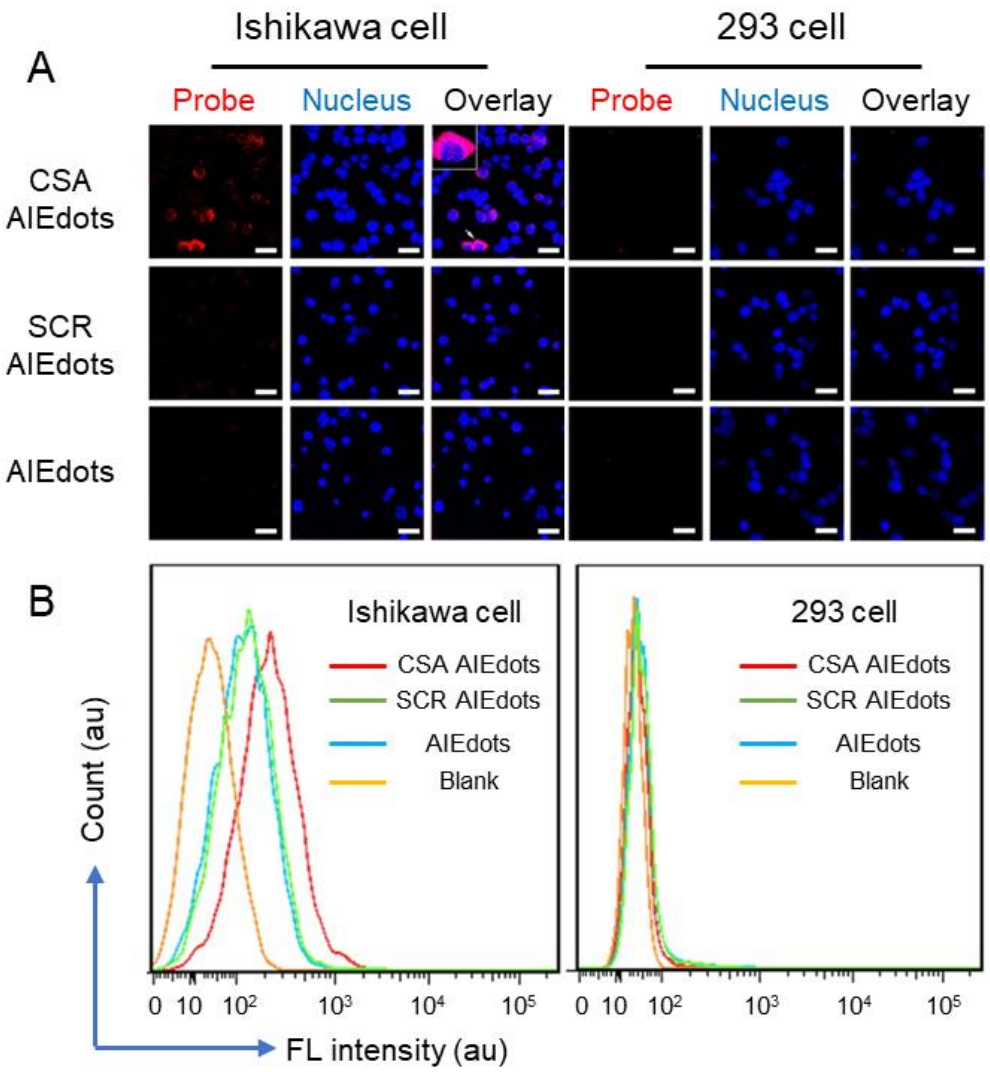
A
Ishikawa cell
293 cell
Probe
Nucleus
Overlay
Probe
Nucleus
Overlay
CSA AIEdots
SCR AIEdots
AIEdots
B
Ishikawa cell
293 cell
CSA AIEdots
SCR AIEdots
AIEdots
Blank
Count (au)
0 10 10² 10³ 10⁴ 10⁵
FL intensity (au)

Figure 4

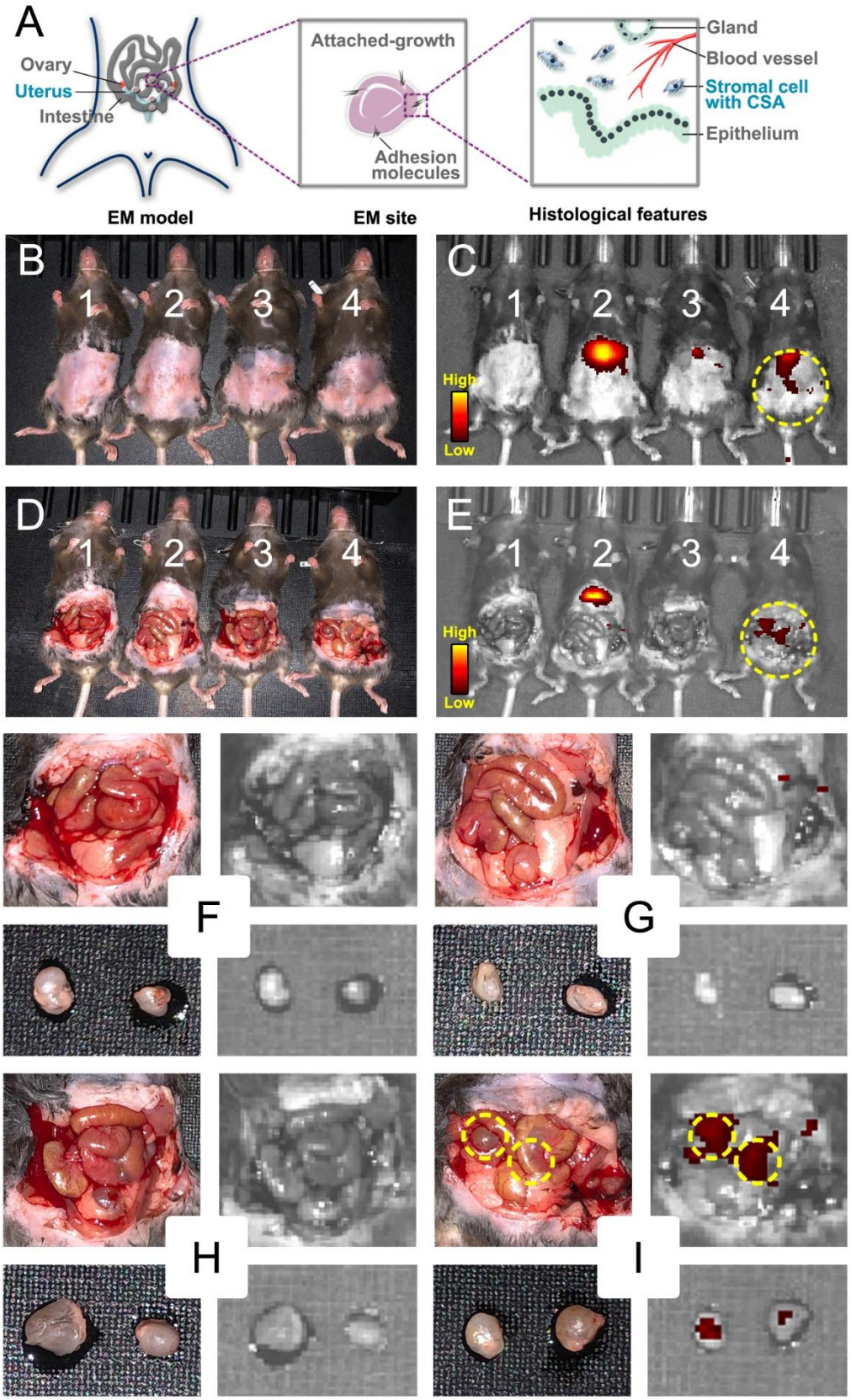
A
Ovary
Uterus
Intestine
Attached-growth
Adhesion molecules
Gland
Blood vessel
Stromal cell with CSA
Epithelium
EM model
EM site
Histological features
B
C
D
E
1
2
3
4
High
Low
F
G
H
I

Figure 5

References

1. Mehedintu, C.; Plotogea, M. N.; Ionescu, S.; Antonovici, M., *Journal of medicine and life* **2014,** *7* (3), 349-57.
2. Dinulescu, D. M.; Ince, T. A.; Quade, B. J.; Shafer, S. A.; Crowley, D.; Jacks, T., *Nature medicine* **2005,** *11* (1), 63-70. DOI 10.1038/nm1173.
3. Giudice, L. C., *The New England journal of medicine* **2010,** *362* (25), 2389-98. DOI 10.1056/NEJMcp1000274.
4. Bacci, M.; Capobianco, A.; Monno, A.; Cottone, L.; Di Puppo, F.; Camisa, B.; Mariani, M.; Brignole, C.; Ponzoni, M.; Ferrari, S.; Panina-Bordignon, P.; Manfredi, A. A.; Rovere-Querini, P., *The American journal of pathology* **2009,** *175* (2), 547-56. DOI 10.2353/ajpath.2009.081011.
5. Tal, A.; Tal, R.; Pluchino, N.; Taylor, H. S., *Biology of reproduction* **2019,** *100* (6), 1453-1460. DOI 10.1093/biolre/ioz039.
6. Klemmt, P. A. B.; Starzinski-Powitz, A., *Curr Womens Health Rev* **2018,** *14* (2), 106-116. DOI 10.2174/1573404813666170306163448.
7. Macer, M. L.; Taylor, H. S., *Obstet Gynecol Clin North Am* **2012,** *39* (4), 535-49. DOI 10.1016/j.ogc.2012.10.002.
8. Rolla, E., *F1000Research* **2019,** *8*. DOI 10.12688/f1000research.14817.1.
9. Wykes, C. B.; Clark, T. J.; Khan, K. S., *BJOG : an international journal of obstetrics and gynaecology* **2004,** *111* (11), 1204-12. DOI 10.1111/j.1471-0528.2004.00433.x.
10. Hsu, A. L.; Khachikyan, I.; Stratton, P., *Clinical obstetrics and gynecology* **2010,** *53* (2), 413-9. DOI 10.1097/GRF.0b013e3181db7ce8.
11. Mondal, S. B.; Gao, S.; Zhu, N.; Liang, R.; Gruev, V.; Achilefu, S., *Adv Cancer Res* **2014,** *124*, 171-211. DOI 10.1016/B978-0-12-411638-2.00005-7.
12. Michalet, X.; Pinaud, F. F.; Bentolila, L. A.; Tsay, J. M.; Doose, S.; Li, J. J.; Sundaresan, G.; Wu, A. M.; Gambhir, S. S.; Weiss, S., *Science* **2005,** *307* (5709), 538-44. DOI 10.1126/science.1104274.
13. Liu, Z.; Peng, R., *Eur J Nucl Med Mol Imaging* **2010,** *37 Suppl 1*, S147-63. DOI 10.1007/s00259-010-1452-y.
14. Qin, W.; Ding, D.; Liu, J. Z.; Yuan, W. Z.; Hu, Y.; Liu, B.; Tang, B. Z., *Adv Funct Mater* **2012,** *22* (4), 771-779.
15. Zhu, C.; Kwok, R. T. K.; Lam, J. W. Y.; Tang, B. Z., *ACS Applied Bio Materials* **2018,** *1* (6), 1768-1786. DOI 10.1021/acsabm.8b00600.
16. Feng, G.; Liu, B., *Accounts of Chemical Research* **2018,** *51* (6), 1404-1414. DOI 10.1021/acs.accounts.8b00060.
17. Lou, X. D.; Zhao, Z. J.; Tang, B. Z., *Small* **2016,** *12* (47), 6430-6450.
18. Feng, G. X.; Liu, B., *Small* **2016,** *12* (47), 6528-6535.
19. Liu, J.; Chen, C.; Ji, S. L.; Liu, Q.; Ding, D.; Zhao, D.; Liu, B., *Chem Sci* **2017,** *8* (4), 2782-2789.
20. Ni, X.; Zhang, X.; Duan, X.; Zheng, H.-L.; Xue, X.-S.; Ding, D., *Nano Letters* **2019,** *19* (1), 318-330. DOI 10.1021/acs.nanolett.8b03936.
21. Ni, X.; Zhang, X.; Duan, X.; Zheng, H. L.; Xue, X. S.; Ding, D., *Nano Lett* **2019,** *19* (1), 318-330. DOI 10.1021/acs.nanolett.8b03936.
22. Du, J.; Liu, S.; Zhang, P.; Liu, H.; Li, Y.; He, W.; Li, C.; Chau, J. H. C.; Kwok, R. T. K.; Lam, J. W. Y.; Cai, L.; Huang, Y.; Zhang, W.; Hou, J.; Tang, B. Z., *ACS applied materials & interfaces* **2020,** *12* (7), 8040-8049. DOI 10.1021/acsami.9b22957.
23. Moses, A. S.; Demessie, A. A.; Taratula, O.; Korzun, T.; Slayden, O. D.; Taratula, O., *Small* **2021**, e2004975. DOI 10.1002/smll.202004975.
24. Moses, A. S.; Taratula, O. R.; Lee, H.; Luo, F.; Grenz, T.; Korzun, T.; Lorenz, A. S.; Sabei, F. Y.; Bracha, S.; Alani, A. W. G.; Slayden, O. D.; Taratula, O., *Small* **2020,** *16* (18), e1906936. DOI 10.1002/smll.201906936.
25. Ahn, S. H.; Singh, V.; Tayade, C., *Fertility and sterility* **2017,** *107* (3), 523-532. DOI 10.1016/j.fertnstert.2017.01.009.

26. Ek, M.; Roth, B.; Engstrom, G.; Ohlsson, B., *Int J Mol Sci* **2019,** *20* (1). DOI 10.3390/ijms20010189.
27. Fassbender, A.; Burney, R. O.; O, D. F.; D'Hooghe, T.; Giudice, L., *BioMed research international* **2015,** *2015*, 130854. DOI 10.1155/2015/130854.
28. Burney, R. O., *Scand J Clin Lab Invest Suppl* **2014,** *244*, 75-81; discussion 80. DOI 10.3109/00365513.2014.936692.
29. May, K. E.; Conduit-Hulbert, S. A.; Villar, J.; Kirtley, S.; Kennedy, S. H.; Becker, C. M., *Human reproduction update* **2010,** *16* (6), 651-74. DOI 10.1093/humupd/dmq009.
30. Hickey, M.; Ballard, K.; Farquhar, C., *Bmj* **2014,** *348*, g1752. DOI 10.1136/bmj.g1752.
31. Srivastava, A.; Gangnard, S.; Round, A.; Dechavanne, S.; Juillerat, A.; Raynal, B.; Faure, G.; Baron, B.; Ramboarina, S.; Singh, S. K.; Belrhali, H.; England, P.; Lewit-Bentley, A.; Scherf, A.; Bentley, G. A.; Gamain, B., *Proceedings of the National Academy of Sciences of the United States of America* **2010,** *107* (11), 4884-9. DOI 10.1073/pnas.1000951107.
32. Salanti, A.; Staalsoe, T.; Lavstsen, T.; Jensen, A. T.; Sowa, M. P.; Arnot, D. E.; Hviid, L.; Theander, T. G., *Mol Microbiol* **2003,** *49* (1), 179-91. DOI 10.1046/j.1365-2958.2003.03570.x.
33. Salanti, A.; Dahlback, M.; Turner, L.; Nielsen, M. A.; Barfod, L.; Magistrado, P.; Jensen, A. T.; Lavstsen, T.; Ofori, M. F.; Marsh, K.; Hviid, L.; Theander, T. G., *The Journal of experimental medicine* **2004,** *200* (9), 1197-203. DOI 10.1084/jem.20041579.
34. Zhang, B.; Liang, R.; Zheng, M.; Cai, L.; Fan, X., *Int J Mol Sci* **2019,** *20* (15). DOI 10.3390/ijms20153642.
35. Yasuo, T.; Yamaguchi, T.; Kitaya, K., *The Journal of steroid biochemistry and molecular biology* **2010,** *122* (4), 159-63. DOI 10.1016/j.jsbmb.2010.07.004.
36. Zhang, B.; Tan, L.; Yu, Y.; Wang, B.; Chen, Z.; Han, J.; Li, M.; Chen, J.; Xiao, T.; Ambati, B. K.; Cai, L.; Yang, Q.; Nayak, N. R.; Zhang, J.; Fan, X., *Theranostics* **2018,** *8* (10), 2765-2781. DOI 10.7150/thno.22904.
37. Pal, D.; Saha, S., *RSC Advances* **2019,** *9* (48), 28061-28077. DOI 10.1039/C9RA05546K.
38. Resende, M.; Nielsen, M. A.; Dahlback, M.; Ditlev, S. B.; Andersen, P.; Sander, A. F.; Ndam, N. T.; Theander, T. G.; Salanti, A., *Malar J* **2008,** *7*, 104. DOI 10.1186/1475-2875-7-104.
39. Khunrae, P.; Dahlback, M.; Nielsen, M. A.; Andersen, G.; Ditlev, S. B.; Resende, M.; Pinto, V. V.; Theander, T. G.; Higgins, M. K.; Salanti, A., *Journal of molecular biology* **2010,** *397* (3), 826-34. DOI 10.1016/j.jmb.2010.01.040.
40. Beeson, J. G.; Rogerson, S. J.; Cooke, B. M.; Reeder, J. C.; Chai, W.; Lawson, A. M.; Molyneux, M. E.; Brown, G. V., *Nature medicine* **2000,** *6* (1), 86-90. DOI 10.1038/71582.
41. Agerbaek, M. O.; Bang-Christensen, S. R.; Yang, M. H.; Clausen, T. M.; Pereira, M. A.; Sharma, S.; Ditlev, S. B.; Nielsen, M. A.; Choudhary, S.; Gustavsson, T.; Sorensen, P. H.; Meyer, T.; Propper, D.; Shamash, J.; Theander, T. G.; Aicher, A.; Daugaard, M.; Heeschen, C.; Salanti, A., *Nature communications* **2018,** *9* (1), 3279. DOI 10.1038/s41467-018-05793-2.
42. Berardo, P. T.; Abrao, M. S.; Souza, M. L.; Machado, D. E.; Silva, L. C.; Nasciutti, L. E., *Micron* **2009,** *40* (5-6), 639-45. DOI 10.1016/j.micron.2009.02.005.